XXXVI Ibero-Latin American Congress on Computational Methods in Engineering
CILAMCE
Rio de Janeiro, 22-25 Nov 2015

ON DENSITY AND GROUND STRUCTURE TOPOLOGY OPTIMIZATION SOLUTIONS TO CONCEPTUAL BUILDING DESIGN

Sara Brandão

Sylvia R. M. Almeida

sarabrandao26@gmail.com

sylvia@ufg.br

Escola de Engenharia Civil, Universidade Federal de Goiás

Av. Universitária, n 1488, Qd86, Setor Universitário, Goiânia, GO, 74605-220, Brasil

Abstract. *Topology optimization provides design solutions to several engineering applications and density methods are the most popular approach in this field. However, when it comes to building design, the dimension of the extended domain related to the high of the building provides material concentration at the basis of the building. On the other side, the ground structure method provides desirable grid solutions using a highly connected truss in a approach close to size optimization techniques. This work presents a prospective study about the application of both density methods and the ground structure method to conceptual design of buildings and explores desirable manufacturing constraints such as patterns repetition and symmetry. Simulations are developed in two-dimensional building configurations, illustrating the potential future applications of this work in the context of building layout optimization.*

Keywords: *Topology optimization, density methods, ground structure, manufacturing constrains.*

1 INTRODUCTION

Topology optimization techniques provide design solutions for a large set of applications. Those techniques were first applied to structural optimization in mechanical engineering and nowadays have been gradually embraced for civil engineering. Several methods in continuum topology optimization field lead to optimal design solutions such as: density-based methods, hard-kill methods, boundary variation methods, bio-inspired cellular division methods (Deaton & Grandhi, 2014). On the other hand, the increase in computational power and mesh generation techniques provide a comprehensive tooling for the use of size optimization inspired techniques such as the ground structure method (Dorn et al., 1964) to generate discrete topological solutions (Zegard & Paulino, 2014).

Density methods search for the optimal layout of a fixed amount of material in a given extended domain. A continuum approach is adopted for the material distribution, although associated to a discretized mesh used in the finite element analysis. On the other hand, the ground structure method provides desirable grid solutions using a highly connected truss. Both continuum and discrete approaches can be used to obtain the layout of lateral bracing systems in high-rise buildings and the discussion on the application of these two approaches to assist the conceptual design of buildings is the main objective of this paper.

It is important to notice that resulting topologies produced by topology optimization often consist of complex geometries of limited value to real world problems. No matter the approach adopted, the design concept is affected by architectural and/or manufacturing issues which are crucial for the layout definition. Therefore, in order to make the results more significant from an engineering perspective, manufacturing controls are introduced to guarantee the construction viability. These desirable features for construction and manufacturing can be controlled by some constraints in the formulation of both density and ground structure methods. Imposing symmetry and pattern repetition conditions in continuum topology optimization were previously explored by Almeida et al (2010) and Stromberg et al (2011). This paper expands the concept applied by Torres e Almeida (2013) to building design in a continuum optimization context to the discrete formulation of the ground structure method an makes comparisons on the results obtained with both techniques.

2 DENSITY METHODS FORMULATION

Density-based methods are the most widely used methodologies for structural topology optimization (Deaton & Grandhi, 2014). By this approach, the classical compliance problem aims to find the material distribution that minimizes the mean compliance of the structure, which conduces to the maxima stiffness. The material density vector $\boldsymbol{\rho}$ is described in terms of the design variables $\mathbf{x}$, where a zero density value indicates a void whereas the unit represents solid material. For generality sake, the structural analysis is carried out using a numerical method, usually the Finite Element (FE) approach. In this paper, the problem is stated in terms of the element densities, ρ_e, and the nodal displacement $\mathbf{U}$, stated as Eq. (1).

$$
\begin{array}{ll}
\text{Find} & \mathbf{y} \\
\text{That minimizes} & c(\mathbf{y}) = \mathbf{U}^{\mathrm{T}}\ \mathbf{K}\ \mathbf{U} \\
\text{Such that :} & \mathbf{K}(\boldsymbol{\rho})\ \mathbf{U} = \mathbf{F} \\
& \sum_{\rho \in \Omega} \rho_e(\mathbf{y})\, v_e = f\ Vol_0 \\
& \rho_e(\mathbf{y}) \in [0,1]
\end{array}
\tag{1}
$$

Here, $\mathbf{y}$ are the design variables, $c(\mathbf{y})$ is the objective function representing the mean compliance of the structure; $\boldsymbol{\rho}$ is the vector containing the element densities $\rho_e(\mathbf{y})$ associated to each finite element *e*; $\mathbf{F}$ is the global nodal force vector; $\mathbf{U}$ is the global displacement vector; $\mathbf{K}$ is the global stiffness matrix.

The formulation based on discrete variables lacks solution in the continuum setting (Sigmund & Petersson, 1998) and thus a relaxation allowing a continuous variation of density is applied. However, simple continuous variation conduces to undesired intermediate densities in the final layout and penalization techniques are used to solve this problem. The SIMP model (Bendsøe, 1989 and Zhou & Rozvany, 1991), described by Eq. (2), is the most widely applied relaxation rule used with density methods in topology optimization.

$$
E(\rho) = \rho^{p}\ E_0 \tag{2}
$$

Where. E is the Young´s modulus for density ρ; E_0 is the Young´s modulus for solid material; and $p \geq 3$ is a penalization parameter.

By the classical element-based approach for topology optimization element density is assumed to be constant within each element. Therefore, the element stiffness matrix $\mathbf{k_e}$ can be evaluated in terms of the stiffness matrix for solid material $\mathbf{k}_0$ as shown in Eq. (3).

$$
\mathbf{k}_e = \rho_e^{\ p}\ \mathbf{k}_0 \tag{3}
$$

The objective function (the mean compliance) can thus be expressed in terms of the element stiffness matrix for solid material as shown in Eq. (4).

$$
c = \sum_{e \in \Omega} \rho_e^{\ p}\ \mathbf{u}_e^{\ T}\ \mathbf{k}_0\ \mathbf{u}_e \tag{4}
$$

The optimization problem is then expressed by Eq. (5), where the minimum value ρ_{min} for ρ_e is adopted to avoid numerical instabilities when solving the equilibrium equations during the FE analysis.

$$
\begin{array}{lll}
\text{Find} & \mathbf{y} & \\
\text{That minimizes} & c(\mathbf{y}) = \sum_{e \in \Omega} \rho_e{}^p \, \mathbf{u}_e{}^T \, \mathbf{k}_0 \, \mathbf{u}_e & \\
\text{Such that :} & \mathbf{K}(\boldsymbol{\rho}) \, \mathbf{U} = \mathbf{F} & (5) \\
 & \sum_{\rho \in \Omega} \rho_e(\mathbf{y}) \, v_e = f \; Vol_0 & \\
 & \rho_{\min} \le \rho_e(\mathbf{y}) \le 1 &
\end{array}
$$

The sensitivity of the objective function from Eq. (4) is evaluated by Eq. (6). For more on this feature see Bendsøe and Sigmund (2003).

$$
\frac{\partial c}{\partial \rho_e} = - \, p \; \rho_e{}^{p-1} \, \mathbf{u}_e{}^T \, \mathbf{k}_0 \, \mathbf{u}_e \tag{6}
$$

Unfortunately topology optimization solutions suffer from several numerical instabilities such as checkerboards phenomenon, mesh dependence and local minima. In structural analysis, mesh-refinement should result in a better finite element modeling of the same optimal structure not in a more detailed and qualitatively different structure. In this context, mesh dependence refers to the problem of not obtaining qualitatively the same solution for different mesh sizes or discretizations (Sigmund & Petersson, 1998). Local minima refers to the problem of obtaining different solutions to the same mesh of a discretized problem when choosing different initial parameters (Sigmund & Petersson, 1998). Checkerboard phenomenon refers to solutions alternating void and solid elements. Díaz and Sigmund (1995) concluded that the checkerboard structure has artificially high stiffness obtained from bad numerical modeling.

Literature presents several techniques to avoid numerical instabilities when using density methods in topology optimization. For density filters, see Guest *et al*. (2004) and Almeida *et al*. (2009), for sensitivity filters see Sigmund (2007) or Sigmund & Petersson (1998). In this paper we use the sensitivity filter, which works by modifying the sensibility of the objective function as shown in Eq. (7).

$$
\frac{\partial \hat{c}}{\partial \rho_e} = \frac{\sum_{f \in R_e} w_f^e \; \rho_f \; \dfrac{\partial c}{\partial \rho_f}}{\rho_e \; \sum_{f \in R_e} w_f^e} \tag{7}
$$

The weight factor w in Eq (7) is a convolution operator described as the distance between the centre of element e (coordinates x_e) and the centre of each element f (coordinates x_f) within region R_e, as shown in Eq. (8). Each region R_e is a circle (2D) or a sphere (3D) of radius r_{min} centered coincident to the centre of element e.

$$w_f^e = \begin{cases} r_{\min} - r_f^e & se \quad x_f \in R_e \\ 0 & se \quad x_f \notin R_e \end{cases} \tag{8}$$

3 GROUND STRUCTURE FORMULATION

The ground structure method (Dorn *et al.*, 1964) provides desirable grid solutions using a highly connected truss in an approach close to size optimization techniques. Unnecessary bars are removed from the truss during the optimization process.

According to Michell (1904), given stress limits in tension $\sigma_T > 0$ and compression $\sigma_C > 0$, and the average limit stress $\sigma_0 = (\sigma_T + \sigma_C)/2$, a truss is optimal if: the truss is in equilibrium; the stress at each member is equal to either σ_T (stress limits in tension) or σ_C (stress limits in compression) for all members; and there exists a compatible deformation field. Thus, the members in the resulting structure are arranged in the directions of the principal strains for the displacement field.

The elastic formulation is based on stiffness and displacements that satisfy the compatibility equations. Considering therefore a rigid truss and assuming that the supports are sufficient to avoid the structure from having rigid body motions, the basic formulation for the minimum volume truss is then expressed in Eq. (9) (Ohsaki, 2010).

$$\begin{array}{ll} \text{Find} & \mathbf{a} \\ \text{That minimizes} & V = \mathbf{l}^T \ \mathbf{a} \\ \text{Such that} & \mathbf{K}\ \mathbf{U} = \mathbf{F} \\ & -\sigma_C \le \sigma_i \le \sigma_T \\ & a_i \ge 0 \qquad\qquad i = 1, 2, \ldots, N_b \end{array} \tag{9}$$

Here, **a** represents the vector containing the cross sectional areas a_i, **l** represents the vector containing the element lengths l_i; σ_i, are the stress for each element i; **K** is the global stiffness matrix; **U** is the nodal displacement vector; **F** is the nodal force vector; and N_b is the number of bars.

The plastic formulation provided by Kirsh (1993) is presented in Eq. (10) in terms of the nodal equilibrium matrix **B** (size N_{dof} x N_b), built from the directional cosines of the members, and of a vector **n** with the internal axial forces for all members in the ground structure.

$$
\begin{array}{ll}
\text{Find} & \mathbf{a} \\
\text{That minimizes} & V = \mathbf{l}^T \ \mathbf{a} \\
\text{Such that} & \mathbf{B}^T \ \mathbf{n} = \mathbf{F} \\
 & -\sigma_C \ a_i \leq n_i \leq \sigma_T \ a_i \\
 & a_i \geq 0 \qquad\qquad\qquad i = 1, 2, \ldots, N_b
\end{array}
\tag{10}
$$

The stress constraint (in tension or compression) must be active for all members at the optimum point and the stress constraint can be expressed in terms of member force. Thus, one can convert the inequalities into equalities by incorporating slack variables in the stress constraints s_i^+ and s_i^- (Hemp, 1973 and Achtziger, 2007) such that,

$$
a_i = \frac{s_i^{\,+}}{\sigma_T} + \frac{s_i^{\,-}}{\sigma_C}
\tag{11}
$$

$$
n_i = s_i^{\,+} - s_i^{\,-}
\tag{12}
$$

By introducing Eq. (11) and Eq. (12), the problem presented in Eq. (10) is thus solved as presented in Eq. (13).

$$
\begin{array}{ll}
\text{Find} & \mathbf{s}^+, \mathbf{s}^- \\
\text{That minimize} & \bar{V} = \mathbf{l}^T \left(\dfrac{\mathbf{s}^+}{\sigma_T} + \dfrac{\mathbf{s}^-}{\sigma_C} \right) \\
\text{Such that} & \mathbf{B}^\mathbf{T} \left(\mathbf{s}^+ + \mathbf{s}^- \right) = \mathbf{F} \\
 & s_i^+, s_i^- \geq 0
\end{array}
\tag{13}
$$

This work uses a Matlab code provided by Zégard and Paulino (2014) and modified by the authors to generate the ground structure and obtain the optimal structure. The user defined connectivity level determines the level of redundancy. If two nodes belong to the same element in the base mesh, then they are considered neighbors. From this idea the connectivity level can be explained as follows:

Level 1 connectivity will generate members between all neighboring nodes;

Level 2 connectivity will generate members up to the neighbors of the neighbors;

Level 3 connectivity will generate members up to the neighbors of the neighbors of the neighbors.

4 MANUFACTURING CONSTRAINTS

Topology optimization is a preliminary tool to provide preliminary design solutions. In this context, manufacturing control is relevant and necessary to extend topology optimization solutions to practical applications. Manufacturing constraints such as symmetry and pattern repetition were presented by Almeida *et al*. (2010) to obtain topology optimization solutions using density methods. This paper extends this concept to the ground structure method.

4.1 Symmetry and pattern constraints in density methods

Symmetric and/or patterned layouts in density methods are obtained disclosing the set of element densities (**ρ**) from the set of design variables (**y**). These constraints are introduced by mapping the design variables **y** onto the set of element densities **ρ** applied to various regions of the extended domain. Thus, the set of element densities **ρ** is divided in two subsets: the primary densities $\boldsymbol{\rho}^1$ and the secondary subset $\boldsymbol{\rho}^2$ that is obtained mapping the design variables of subset $\boldsymbol{\rho}^1$.

Figure 1 illustrates the scheme to obtain 2D patterned solutions. The design variables are represented in Figure 1a, the subset $\boldsymbol{\rho}^1$ is represented by the green region and the subset $\boldsymbol{\rho}^2$ by the blue region in Figure 1b. Finally, Figure 1c shows the spatial distribution of the design variables.

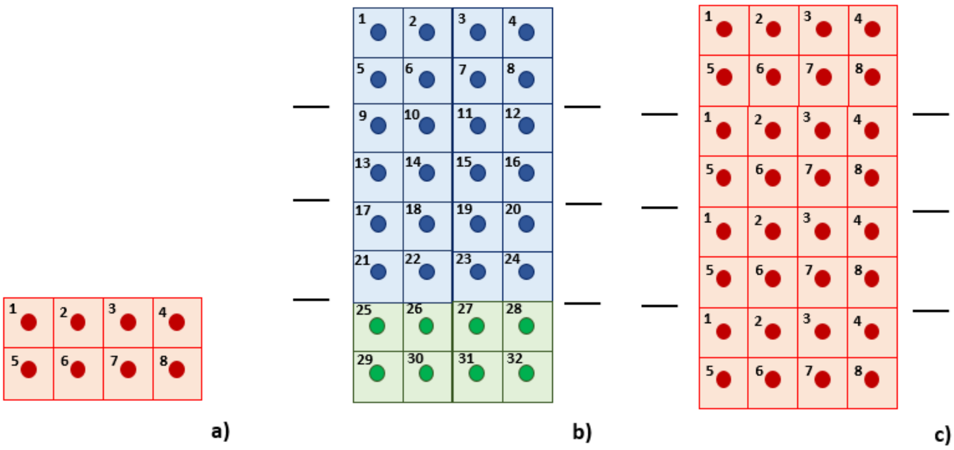

Figure 1 - Mapping of the design variables to achieve pattern repetition along axis *X*

Eq. (14) imposes pattern repetition along axe X and Eq. (15) along axe Y for 2D extended domains. To impose pattern repetition along axes X and Y both equations must be simultaneously applied.

$$\text{if} \quad \begin{cases} X_i = X_j + a \\ Y_i = Y_j \\ Z_i = Z_j \end{cases} \qquad (14)$$

$$\text{then} \quad \rho_i = \rho_j = y_k$$

$$\text{if} \quad \begin{cases} X_i = X_j \\ Y_i = Y_j - b \\ Z_i = Z_j \end{cases} \qquad (15)$$
$$\text{then} \quad \rho_i = \rho_j = y_k$$

This paper expands the formulation presented by Almeida *et al.* (2010) for 3D solutions. Thus, Eq. (16) is added to impose pattern repetition along axe *Z*. To impose pattern repetition along more than one axe the respective equations must be simultaneously applied.

$$\text{if} \quad \begin{cases} X_i = X_j \\ Y_i = Y_j \\ Z_i = Z_j - c \end{cases} \qquad (16)$$
$$\text{then} \quad \rho_i = \rho_j = y_k$$

Where *a*, *b* and *c* represent the dimensions of the patterns along axes *X*, *Y* and *Z*, respectively.

Figure 2 illustrates the scheme to obtain 2D symmetric solutions. The design variables are represented in Figure 2a, the subset $\boldsymbol{\rho}^1$ is represented by the green region and the subset $\boldsymbol{\rho}^2$ by the blue region in Figure 2b. Finally, Figure 2c shows the spatial distribution of the design variables.

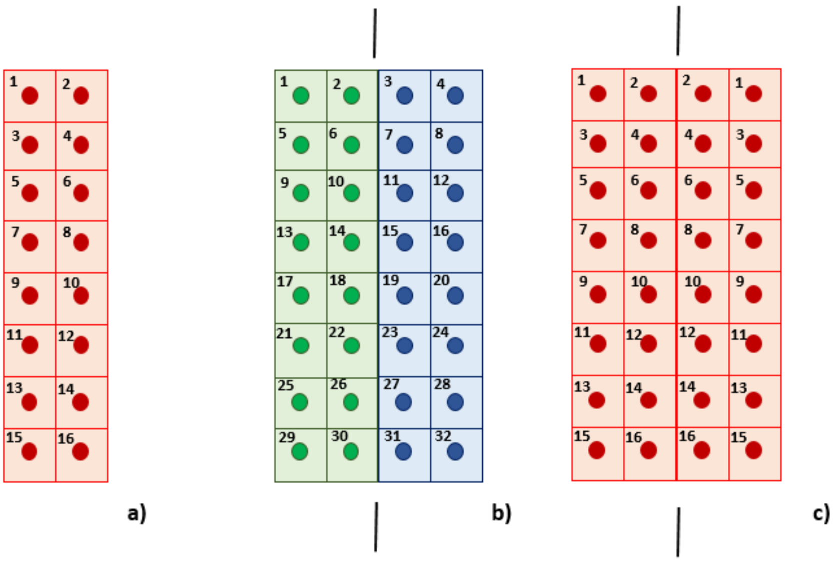

Figure 2 - Mapping of the design variables to achieve symmetry with respect to axis Y

Eq. (17) imposes symmetry with respect to axe *X* and Eq. (18) with respect to axe *Y*. Both equations must be applied to impose symmetry with respect to both axes.

$$\text{if} \quad \begin{cases} X_i = X_j \\ Y_i = L_Y - Y_j \\ Z_i = Z_j \end{cases} \qquad (17)$$
$$\text{then} \quad d_i = d_j = y_k$$

$$\text{if} \quad \begin{cases} X_i = L_X - X_j \\ Y_i = Y_j \\ Z_i = Z_j \end{cases} \qquad (18)$$
$$\text{then} \quad d_i = d_j = y_k$$

To expand the formulation presented by Almeida *et al.* (2010) for 3D solutions, one must apply Eq. (17) to impose symmetry with respect to plan *Y*-*Z* and Eq. (18) with respect to plan *X*-*Z* and Eq. (19) with respect to plan *X*-*Y*. To impose symmetry with respect more than one plan the respective equations must be simultaneously applied.

$$\text{if} \quad \begin{cases} X_i = X_j \\ Y_i = Y_j \\ Z_i = L_Z - Z_j \end{cases} \qquad (19)$$
$$\text{then} \quad d_i = d_j = y_k$$

Where L_X, L_Y and L_Z represent the dimensions of the design domain along axes *X*, *Y* and *Z*, respectively.

4.2 Symmetry and pattern constraints – ground structure methods

The equations developed by Almeida *et al*. (2010) to impose manufacturing control in density methods are here adapted to the ground structure method. The difference is that in ground structure methods the variables are the cross sectional area of the bars. Figure 3 illustrates the scheme to obtain 2D patterned solutions. The design variables are represented in Figure 3a, the subset $\mathbf{a}^1$ is represented by the green bars and the subset $\mathbf{a}^2$ by the blue bars in Figure 3b. Finally, Figure 3c shows the spatial distribution of the design variables.

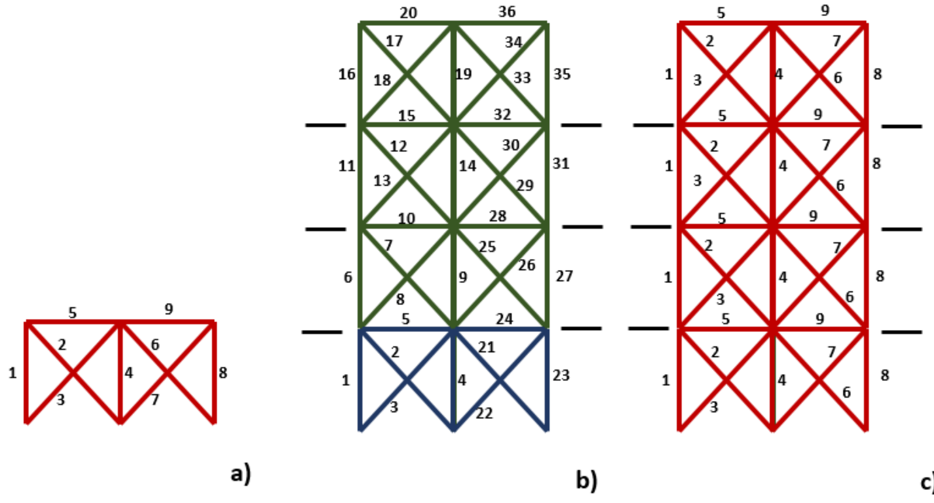

Figure 3 - Mapping of the design variables to achieve pattern repetition along axes X

In 3D applications, Eq. (20) imposes pattern repetition with respect to plan *Y*-*Z*, Eq. (21) with respect to plan *X*-*Z* and Eq. (22) with respect to plan X-*Y*. To impose pattern repetition along more than one axe the respective equations must be simultaneously applied.

$$\text{if} \quad \begin{cases} X_{1i} = X_{1j} + a \\ X_{2i} = X_{2j} + a \\ Y_{1i} = Y_{1j} \\ Y_{2i} = Y_{2j} \\ Z_{1i} = Z_{1j} \\ Z_{2i} = Z_{2j} \end{cases} \qquad \text{then} \quad A_i = A_j = y_k \tag{20}$$

$$\text{if} \quad \begin{cases} X_{1i} = X_{1j} \\ X_{2i} = X_{2j} \\ Y_{1i} = Y_{1j} - b \\ Y_{2i} = Y_{2j} - b \\ Z_{1i} = Z_{1j} \\ Z_{2i} = Z_{2j} \end{cases} \qquad \text{then} \quad A_i = A_j = y_k \tag{21}$$

$$\text{if}\quad \begin{cases} X_{1i} = X_{1j} \\ X_{2i} = X_{2j} \\ Y_{1i} = Y_{1j} \\ Y_{2i} = Y_{2j} \\ Z_{1i} = Z_{1j} - c \\ Z_{2i} = Z_{2j} - c \end{cases} \qquad (22)$$
$$\text{then}\quad A_i = A_j = y_k$$

Figure 4 illustrates the scheme to obtain 2D symmetric solutions. The design variables are represented in Figure 4a, the subset $\mathbf{a}^1$ is represented by the green bars and the subset $\mathbf{a}^2$ by the blue bars in Figure 4b. Finally, Figure 4c shows the spatial distribution of the design variables.

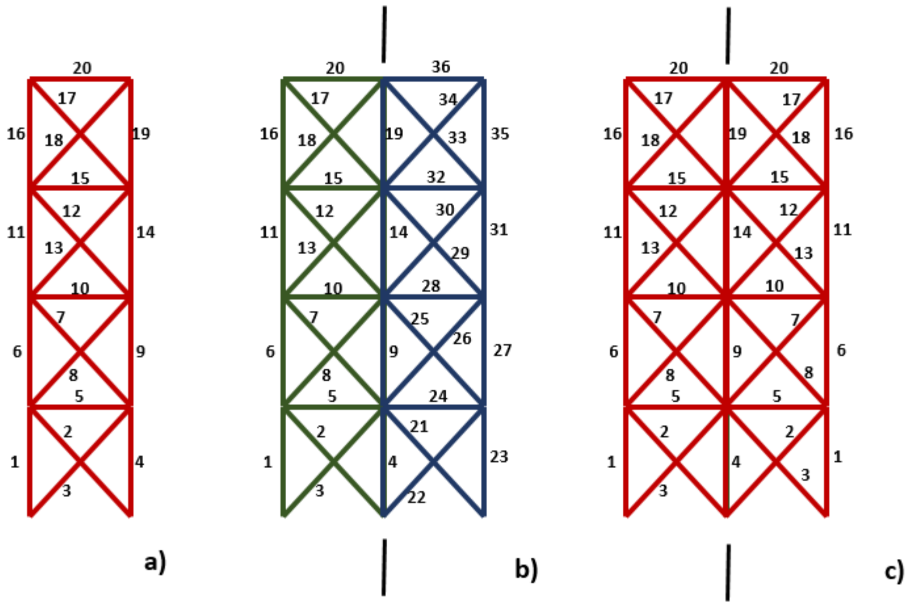

Figure 4 - Mapping of the design variables to achieve symmetry with respect to axis Y

In 3D applications, Eq. (23) imposes symmetry with respect to plan *Y-Z*, Eq. (24) with respect to plan *X-Z* and Eq. (25) with respect to plan X-*Y*. To impose pattern repetition along more than one axe the respective equations must be simultaneously applied.

$$\text{if} \quad \begin{cases} X_{1i} = X_{1j} \\ X_{2i} = X_{2j} \\ Y_{1i} = L_Y - Y_{1j} \\ Y_{2i} = L_Y - Y_{2j} \\ Z_{1i} = Z_{1j} \\ Z_{2i} = Z_{2j} \end{cases} \quad \text{then} \quad A_i = A_j = y_k \tag{23}$$

$$\text{if} \quad \begin{cases} X_{1i} = L_X - X_{1j} \\ X_{2i} = L_X - X_{2j} \\ Y_{1i} = Y_{1j} \\ Y_{2i} = Y_{2j} \\ Z_{1i} = Z_{1j} \\ Z_{2i} = Z_{2j} \end{cases} \quad \text{then} \quad A_i = A_j = y_k \tag{24}$$

$$\text{if} \quad \begin{cases} X_{1i} = X_{1j} \\ X_{2i} = X_{2j} \\ Y_{1i} = Y_{1j} \\ Y_{2i} = Y_{2j} \\ Z_{1i} = L_Z - Z_{1j} \\ Z_{2i} = L_Z - Z_{2j} \end{cases} \quad \text{then} \quad A_i = A_j = y_k \tag{25}$$

5 NUMERICAL RESULTS

This section addresses the problem of a 288 m tall building in Australia presented in Beghini *et al*. (2014) and presented in Figure 5a. In this paper, two different forms of lateral loads are analyzed. The first load, presented in Figure 5b, is a point horizontal force at the top of the building. The second load, presented in Figure 5c is a distributed lateral load.

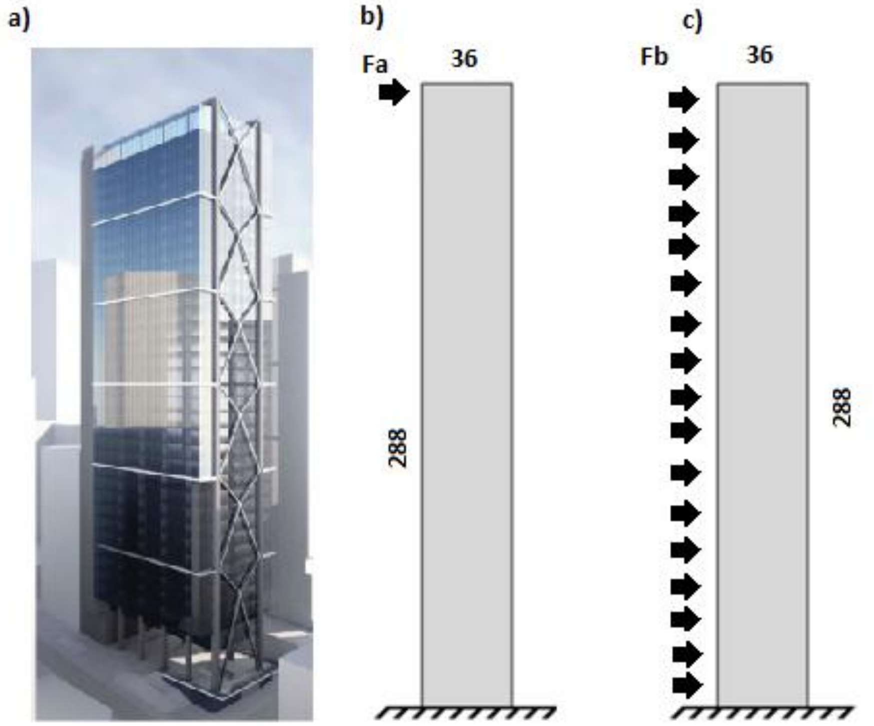

Figure 5 - a) 288 m tall building; b) concetrated load; c) distributed load

5.1 Results using density methods

All examples are run using penalization factor p = 3 and r_{min} = 1.5 elements. The design domain is discretized in a mesh of 36 x 288 Q4 elements. Symmetry constraints were imposed with respect to the vertical axe.

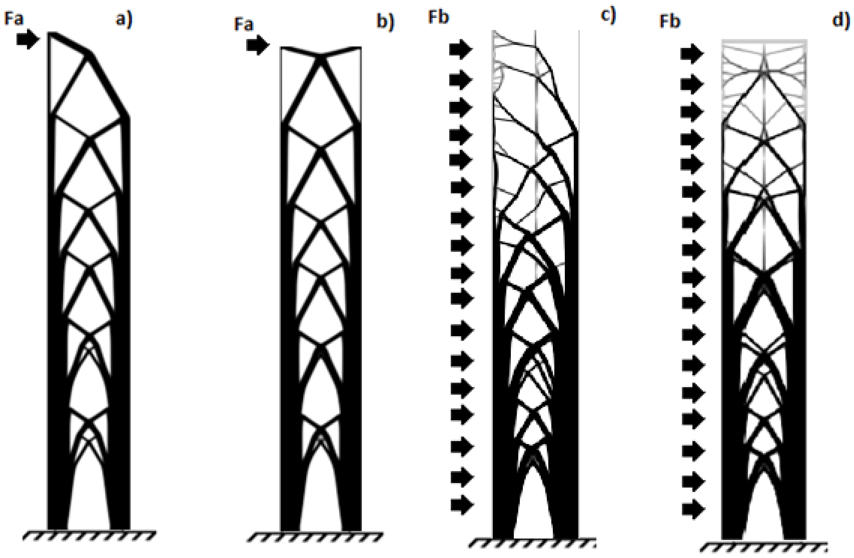

Figure 6 – Solutions using density method: a) Solution for concentrated load without manufacturing constraints; b) Solution for concentrated load applying symmetry constraints; c) Solution for distributed load without manufacturing constraints; d) Solution for distributed load with symmetry applying symmetry constraints

Figure 6a and 6b presents the topology optimization results obtained applying only a lateral unitary load. In this the material distribution is homogeneous. Figure 6.c, 6.d presents the topology results obtained by a distributed lateral load, where the material distribution is concentrated in the base of the building. The results show a material concentration near to the ground due to the vertical dimension of the building, which is much bigger than the horizontal dimension, and the support conditions. Intermediate densities can also be observed at the top of the building, specially for the distributed load, which is closer to the actual design condition. Such solutions are not fit to practical applications in design process.

5.2 Results using the ground structure method

The ground structure method is run using a mesh with 2 x 16 bar elements and the simulation of the distributed load is carried out by applying several point loads along the vertical edge.

Figure 7 shows the results for connectivity levels 1 and 2 obtained with no manufacturing constraint. The grid solutions obtained can easily be applied to actual design solutions. The application of several point loads induces more bars to be maintained in the final solutions for connectivity level 1. This effect is not observed when adopting connectivity level 2;

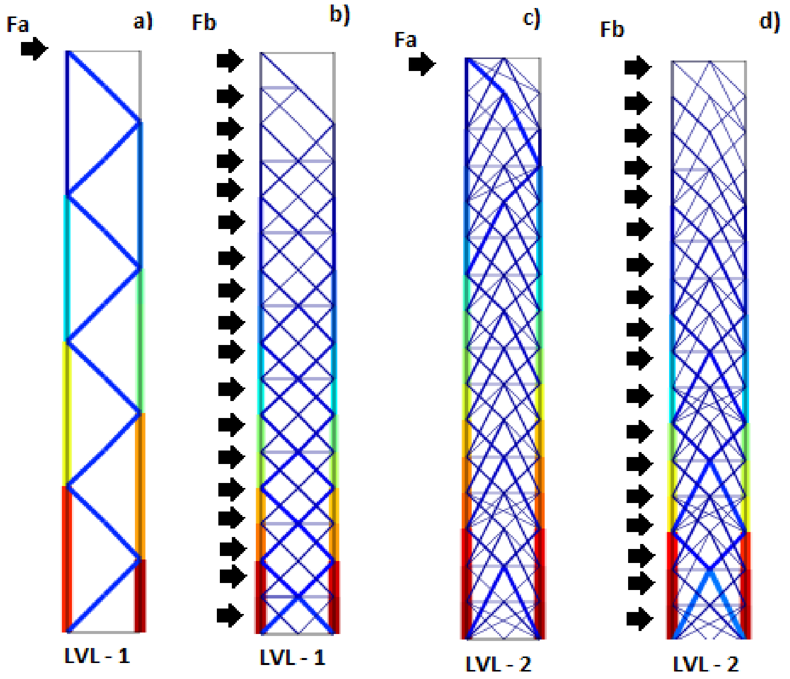

Figure 7 - Solutions using the ground structure method: a) Concentrated load - Lvl 1; b) Distributed load - Lvl 1; c) Concentrated load - Lvl 2; d) Distributed load - Lvl 2

Figure 8 shows the results for connectivity levels 1 and 2 obtained applying symmetry constraints with respect to axis *Y*. The solution for the point load and connectivity level 1 is not applicable in actual design.

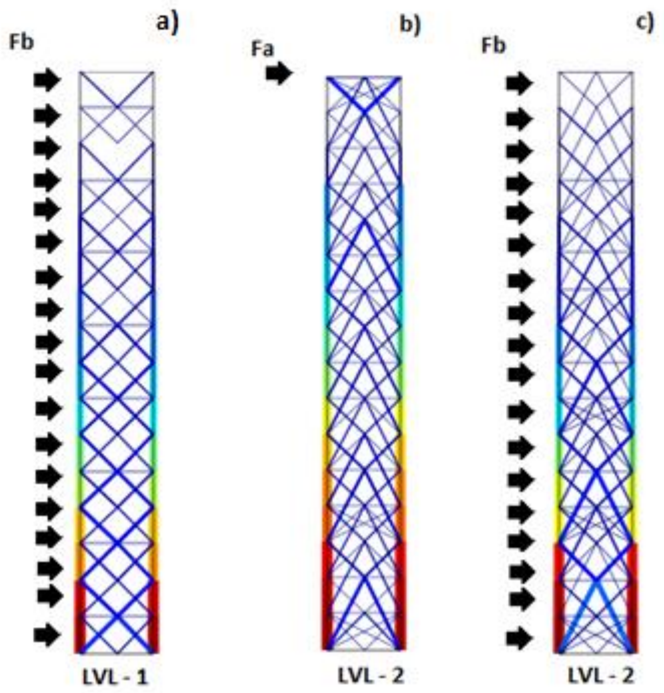

Figure 8 - Solutions using the ground structure method: a) Distributed load - Lvl 1 - Symmetry; b) Concetrated load - Lvl 2 - Symmetry; c) Distributed load - Lvl 2 - Symmetry

Figure 9 shows the results for connectivity level 1 obtained applying both symmetry and pattern repetition. The solution for the point load is not applicable in actual design.

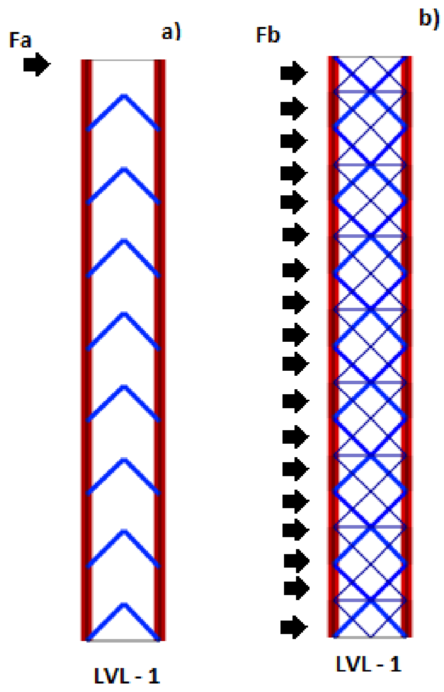

Figure 9 - Solutions using the ground structure method: a) Concetrated load - Lvl 1 - Symmetry and Pattern repetition; b) Distributed load - Lvl 1 - Symmetry and Pattern repetition

This paper presents 3D solutions obtained using the ground structure method, run using a mesh with 2 x 2 x 16 bar elements (Figure 10.a). The first load (Figure 10.b) is a concentrated lateral load. The second load (Figure 10.c) is a distributed lateral load. The third load (Figure 10.d) is a variable load as shown.

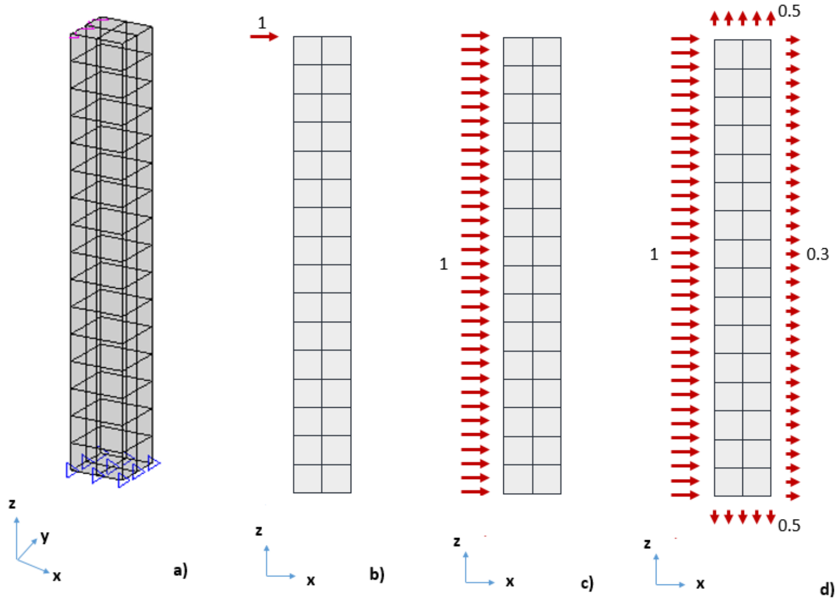

Figure 10 - Solutions using the ground structure method: a) 3D Mesh; b) 3D Concetrated Load; c) 3D Distributed Load; d) 3D Variable Load

Figure 11 shows the results for connectivity level 1 for concentrated load without manufacturing control. Figure 11.a shows the 3D view, 11.b shows de plan X-Z, 11.c shows the plan Y-Z and 11.d shows the plan X-Y.

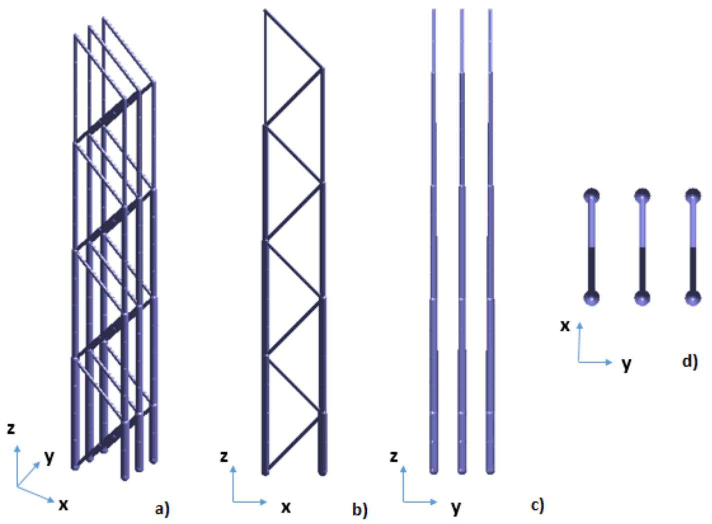

Figure 11 - Solutions using the ground structure method: a) 3D view for concentrated Load Lvl 1; b) Plan X-Z; c) Plan Y-Z; d)Plan X-Y

Figure 12 shows the results for connectivity level 1 for distributed load without manufacturing constraints. Figure 12.a shows the 3D view, 12.b shows de plan X-Z, 12.c shows the plan Y-Z and 12.d shows the plan X-Y.

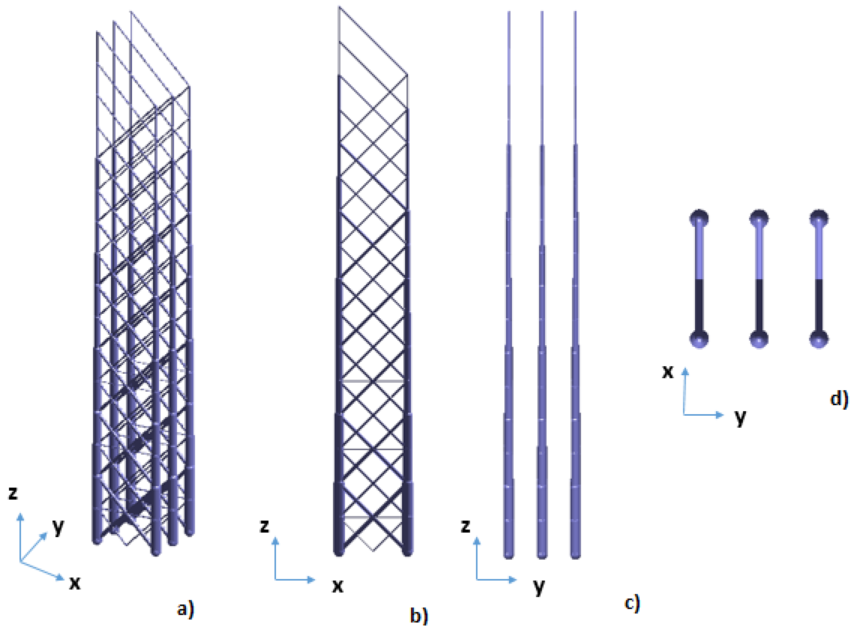

Figure 12 - Solutions using the ground structure method: a) 3D view for distributed Load Lvl 1; b) Plan X-Z; c) Plan Y-Z; d)Plan X-Y

Figure 13 shows the results for connectivity level 1 for variable load without manufacturing control. Figure 13.a shows the 3D view, 13.b shows de plan X-Z, 13.c shows the plan Y-Z and 13.d shows the plan X-Y.

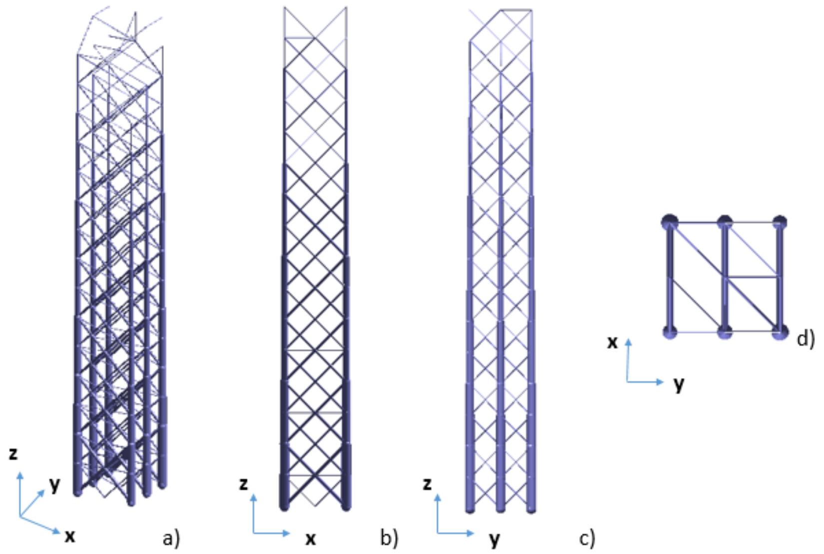

Figure 13 - Solutions using the ground structure method: a) 3D view for variable Load Lvl 1; b) Plan X-Z; c) Plan Y-Z; d)Plan X-Y

6 CONCLUSIONS

This work presented a preliminary study on topology optimization based on density methods and on the ground structure method applied to conceptual building design. Results show that density methods do not provide good design solutions when the design domain has a predominant dimension in one direction and support conditions concentrated in on side of this dimension. In this context, results shows that the ground structure method can be a good alternative to provide topology optimization solutions to high-rise buildings. The grid solutions obtained are closer to the solutions usually adopted by structural designers. Moreover, symmetry and pattern repetition are necessary to lead to a solution with practical applicability in 2D or in 3D applications.

REFERENCES

Achtziger, W., 2007. On simultaneous optimization of truss geometry and topology. *Structural and Multidisciplinary Optimization*, vol. 33, n.4-5, pp. 285-304.

Almeida, S. R. M., & Paulino, G. H., & Silva, E. C. N., 2009. A simple and effective inverse projection scheme for void distribution control in topology optimization. *Structural and Multidisciplinary Optimization*, vol. 39, n.4, pp. 359-371.

Almeida, S. R. M., & Paulino, G. H., & Silva, E. C. N., 2010. Layout and material gradation in topology optimization of functionally graded structures: a global – local approach. *Structural and Multidisciplinary Optimization*, vol.42, n.4, pp. 855-868.

Beghini, L. L., & Beghini, A., & Katz, N., & Baker, W. F., & Paulino, G. H., 2014. Connecting architecture and engineering through structural topology optimization. *Engineering Structures,* vol.59, n.1, pp. 718-726.

Bendsøe, M. P., 1989. Optimal shape design as a material distribution problem. *Structural Optimization,* vol. 1, n. 4, pp. 193-202.

Bendsøe, M. P., & Sigmund, O., 2003. Topology optimization: theory, methods, and applications. Springer.

Deaton, J. D., & Grandhi, R. V., 2015. A survey of structural and multidisciplinary continuum topology optimization: post 2000. *Structural and Multidisciplinary Optimization,* vol. 49, n.1, pp. 1-38.

Díaz, A., & Sigmund, O., 1995. Checkerboard patterns in layout optimization. *Structural and Multidisciplinary Optimization,* vol. 10, n.1, pp. 40-45.

Dorn, W., & Gomory, R., & Greenberg, H., 1964. Automatic design of optimal structures. *J Mecanique,* vol. 3, n.1 , pp 25-52.

Guest, J. K., & Prévost, J. H., & Belytschko, T., 2004. Achieving minimum length scale in topology optimization using nodal design variables and projection functions. *International Journal for Numerical Methods in Engineering,* vol. 61, n. 2, pp 238-254.

Hemp, W., 1973. *Optimum structures.* Oxford university press.

Kirsch, U., 1993. *Structural optimization: fundamentals and applications*. Springer.

Michell, A. G. M., 1904. The limits of economy of material in frame-structures. *Phil Mar Ser*, vol. 47, n. 1, pp 589-597.

Ohsaki, M., 2010. Optimization of finite dimensional structures. CRC Press.

Sigmund, O., 2007. Morphology-based black and white filters for topology optimization. *Structural and Multidisciplinary Optimization*, vol. 33, n.4-5, pp. 401-424.

Sigmund, O., & Petersson, J., 1998. Numerical instabilities in topology optimization: a survey on procedures dealing with checkerboards, mesh-dependencies and local-minima. *Structural and Multidisciplinary Optimization*, vol. 16, n.1, pp. 68-75.

Stromberg, L. L., & Beghini, A., & Baker, W. F., & Paulino, G. H., 2011. Application of layout and topology optimization using pattern gradation for the conceptual design of buildings. *Structural and Multidisciplinary Optimization*, vol. 43, n.1, pp. 165-180.

Torres, I. A., & Almeida, S. R. M., 2013. On conceptual design of building based on topology optimization techniques. In del Prado Z. J. G. N., eds, *XXXIV Iberian Latin American Congress on Computational Methods in Engineering.*

Zegard. T., & Paulino, G. H., 2014. GRAND – Ground structure based topology optimization for arbitrary 2D domains using MATLAB. *Structural and Multidisciplinary Optimization*, vol. 50, n.1, pp. 861-882.

Zhou, M., & Rozvany, G. I. N., 1991. The COC algorithm, part II: topological, geometrical and generalized shape optimization. *Computer Methods in Applied Mechanics and Engineering*, vol. 89, n. 1-3, pp. 309-336.